Article (refereed) - postprint

Martin, R.S.; Wheeler, J.C.; Ilyinskaya, E.; Braban, C.F.; Oppenheimer, C. 2012 The uptake of halogen (HF, HCl, HBr and HI) and nitric (HNO3) acids into acidic sulphate particles in quiescent volcanic plumes. *Chemical Geology*, 296-297. 19-25. 10.1016/j.chemgeo.2011.12.013

The uptake of halogen (HF, HCl, HBr and HI) and nitric (HNO_3) acids into acidic sulphate particles in quiescent volcanic plumes

RS Martin[1], JC Wheeler[1], E Ilyinskaya[2], CF Braban[3] and C Oppenheimer[1]

[1] Department of Geography, University of Cambridge, Cambridge, UK
[2] Icelandic Meteorological Office, Bustadavegi 9, 150 Reykjavik, Iceland
[3] Centre for Ecology & Hydrology, UK

Published in ***Chemical Geology***

Abstract

The uptake of halogen and nitric acids into acidic sulphate particles has important implications for volcano monitoring and the environmental geochemistry of volcanic emissions. Using the Extended Aerosol Inorganics Model (E-AIM) for HCl, HBr and HNO_3, combined with a simple three-parameter model for HF and HI, we show that equilibrium partitioning of halogen and nitric acids into sulphate particles is maximised at high relative humidity (RH), low temperature, low plume dilution (i.e., near-source) and high SO_4^{2-}/SO_2. The addition of metal chlorides (i.e., NaCl) enhances acidic gas partitioning at high RH, but diminishes acidic gas partitioning at low RH due to a decrease in the water content of particles and the formation of Na sulphate salts. We predict that acidic gas partitioning is quantitatively significant (>1%) only in cool humid conditions (e.g., >80% RH at 298 K), adding confidence to spectroscopic and/or electrochemical determinations of gas ratios (e.g., SO_2/HCl, HCl/HF) for volcano monitoring. However, acidic gas partitioning remains environmentally important over a wide range of conditions because of the significant variability in the amounts of acidic gases in particle form (Cl^-(aq), Br^-(aq), I^-(aq), NO_3^-(aq), HF(aq)). This may result in diurnal and seasonal changes in acidic gas deposition downwind of the volcano.

Keywords: volcanic plume, equilibrium model, masaya, E-AIM

1 Introduction

Active volcanoes are a major source of gases and particles to the atmosphere. A significant contribution to global volcanic emissions comes from persistent degassing from volcanoes such as Mt Etna (Sicily) and Masaya (Nicaragua). The activity at these volcanoes is characterised by the sustained emission of volatile species (forming a quiescent volcanic plume) punctuated by sporadic and typically minor eruptions. Volcanic gases are composed of > 90% H_2O and CO_2, and < 10% SO_2, HCl and HF, with smaller and variable amounts of H_2S, H_2, CO, HBr and HI (Gerlach, 2004; Pyle and Mather, 2009). A common feature of quiescent volcanic plumes is micron-sized sulphate particles, with compositions between the acidic (e.g., H_2SO_4) and metal-rich (primarily $(Na,K)_2SO_4$) end-members (e.g., Mather et al., 2003; Martin et al., 2011) at a molar abundance of $SO_4^{2-}/SO_2 \sim 0.01$.

The uptake of halogen acids (HF, HCl, HBr, HI) into sulphate particles has wide implications in volcanology. The magmatic SO_2/HCl gas ratio plays an important role in eruption forecasting and in understanding volcanic degassing (e.g., Horrocks et al., 1999; Duffell et al., 2003) due to the SO_2/HCl ratio decreasing as the magma becomes more degassed. However, the magmatic SO_2/HCl ratio may be overprinted by preferential HCl uptake into sulphate particles. More generally, if uptake into particles is significant, volcanic emissions of F, Cl, Br and/or I (Pyle and Mather, 2009) may be underestimated if the gas and particle phases are not monitored together (as is often the case). Recent measurements indicate ~1% of total HCl and HF are taken up into particles within the first few minutes after emission (e.g., Mather et al., 2006a; Martin et al., 2008, 2010).

The uptake of halogen acids into particles is also environmentally important because particles have a greater potential for deposition than gases, with the rate of sedimentation increasing with particle size. In fact, uptake may control the extent of local deposition for halogen acids since volcanic plumes tend to be emitted and transported at altitudes above the elevation of the surrounding land. At Mt Etna (Sicily), significant airborne concentrations of particles were measured ~2 km below the plume (Allen et al., 2006), consistent with a number of studies measuring or inferring deposition onto the volcano's flanks (e.g., Aiuppa et al., 2006; Bellomo et al., 2007; Watt et al., 2009). At Masaya volcano

(Nicaragua), the environmental impacts of deposition include acidification of soils and a decrease in vegetation health and diversity (e.g., Delmelle et al., 2002). Uptake may also influence local atmospheric chemistry, due to the enhanced rates of chemical reactions within, or on the surface of, particles. Of special interest is the autocatalytic bromine explosion, which results in the production of reactive Br species (e.g., Br, BrO) and rapid O_3 depletion (Oppenheimer et al., 2006; von Glasow, 2010).

In contrast to the halogen acids, nitric acid (HNO_3) is not thought to be a primary magmatic emission (Mather et al., 2004). Equilibrium models predict that NO is produced when atmospheric N_2 and O_2 are heated to > 1000°C at the vent (Gerlach, 2004; Martin et al., 2006). The minor amounts of NO_2 and HNO_3 formed under such conditions cannot explain measurements of high HNO_3/SO_2 (e.g., 0.02 at Masaya (Nicaragua), 0.05 at Etna (Sicily), Mather et al., 2004; 0.03 at Erebus (Antarctica), Oppenheimer et al., 2010). Instead, it is supposed that NO is oxidised rapidly to HNO_3 at ambient temperature in the volcanic plume (Roberts et al., 2009; Boichu et al., 2011), although the mechanism for this process remains unclear. In any case, HNO_3 uptake will likely promote N deposition and this may be important in N-limited ecosystems (Huebert et al., 1999).

The equilibrium limit of uptake is defined by "partitioning", which may be calculated without reference to any time-dependent (i.e., kinetic) processes. While the thermodynamic Extended Aerosol Inorganics Model (E-AIM; Carslaw et al., 1995; Clegg et al., 1998; Wexler and Clegg, 2002) has been used to predict the equilibrium composition of volcanic aerosol on a case-by-case basis (e.g., Mather et al., 2004; Oppenheimer et al., 2006; Martin et al., 2008; Roberts et al., 2009; Martin et al., 2010), the general features of acidic gas partitioning into acidic sulphate particles have yet to be established. In this study we use E-AIM to investigate the extent of HCl, HBr and HNO_3 partitioning over a wide range of atmospheric (i.e., relative humidity, temperature) and plume (i.e., dilution, composition) conditions. A simple three-parameter model is used to extend these results to HF and HI partitioning. The effects of dissolved Na^+ ions on HCl partitioning are also investigated. These results offer new

insights into the uptake of halogen and nitric acids into acidic sulphate particles, and we discuss a range of implications for volcanology and the environmental geochemistry of volcanic emissions.

2 Methodology

2.1 The equilibrium assumption

Particles in quiescent volcanic plumes are mostly secondary in origin (i.e., non-silicate) and are formed in different temperature regimes (Óskarsson, 1980). The mixing of magmatic and atmospheric gases at the vent (> 700°C) results in cooling and condensation of metal salts (e.g., NaCl, KCl, $CaCl_2$, $MgCl_2$, with smaller amounts of the corresponding fluorides; e.g., Symonds et al., 1992; Symonds and Reed, 1993). Additionally, ~1% of SO_2 is oxidised to hygroscopic SO_3 by atmospheric O_2 at the vent (Mather et al., 2006b). With further cooling (< 338°C), SO_3 reacts with H_2O to form gas-phase H_2SO_4, and subsequently droplets of H_2SO_4. The composition of particles measured at the crater-rim will reflect not only the initial amounts of metal salts and H_2SO_4, but the extent of internal mixing between these types of particles, and the interactions between particles and gases (e.g., H_2O, HF, HCl, HBr, HI, HNO_3). The dynamics of this sequence are, of course, hugely complex, with significant potential for non-equilibrium. Due to the extreme hygroscopicity of H_2SO_4, along with the high abundances of gas-phase H_2SO_4 and H_2O, binary homogenous nucleation of H_2SO_4 and H_2O may occur, in addition to the heterogeneous nucleation of H_2SO_4 onto metal salts. Single particle analyses (e.g., Ammann and Burtscher et al., 1990; Ammann et al., 1993; Toutain et al., 1995; Martin et al., 2008; Moune et al., 2010) show a range of compositions indicating that internal mixing is neither negligible nor complete. Thus, while local equilibrium may be established between gases and particles over timescales as short as a few seconds (Wexler and Seinfeld, 1992), the overall gas and particle composition may remain out of equilibrium.

E-AIM (along with other aerosol thermodynamic models, e.g., ISORROPIA II, Fountoukis and Nenes, 2007) assumes simply that particles are at equilibrium with their surroundings, exist as an internal mixture, and are sufficiently large (> 0.1 μm) that they behave as bulk solids or liquids (i.e.,

the Kelvin effect is negligible). Despite these simplifications, thermodynamic calculations are valuable because they allow the influence of different variables (e.g., temperature, relative humidity, input composition) to be established. Furthermore, if equilibrium has not been attained at the crater-rim, equilibrium may be attained further downwind. It is in these older quiescent plumes that rapid heterogeneous oxidation processes (e.g., the bromine explosion) are thought to occur (e.g., Oppenheimer et al., 2006, 2010; Bobrowksi et al., 2007; Roberts et al., 2009; von Glasow, 2010) so our results have wider relevance.

2.2 Modelling

The variants of E-AIM used are E-AIM1 (Carslaw et al., 1995), which considers the H^+ - SO_4^{2-} - NO_3^- - Cl^- - Br^- - H_2O system over 200 to 330 K, and E-AIM3 (Clegg et al., 1998), which considers the H^+ - Na^+ - SO_4^{2-} - NO_3^- - Cl^- - H_2O system at 298.15 K. Both variants calculate the equilibrium composition for a given relative humidity (RH), temperature (T) and input composition.

Our "standard" input composition is based on a mean of 13 gas and particle analyses made at the crater rim of Masaya volcano (Nicaragua) during a period of quiescent degassing (Martin et al., 2010) (Table 2, n_i; in μmol m^{-3}). SO_4^{2-} and HSO_4^- were not distinguished during the chemical analysis so the sum of these ions is represented by $n_{SO42-(aq,s)}$ in Table 2. This data set was chosen as it is one of the few simultaneous measurements of halogen and nitric acid gases and particles in a quiescent volcanic plume. The total amount of each ion was fixed (i.e., mass balanced) using measurements of the most abundant species for Cl^-, Br^-, NO_3^- and SO_4^{2-} ($n_{HCl(g)}$, $n_{HBr(g)}$, $n_{HNO3(g)}$, $n_{SO42-(aq,s)}$; in mol m^{-3} of air). K^+, Ca^{2+} and Mg^{2+} are not considered within E-AIM3 so these ions were entered as "equivalent" Na^+ (i.e., $n_{Na+*(aq,s)} = n_{Na+(aq,s)} + n_{K+(aq,s)} + 2n_{Mg2+(aq,s)} + 2n_{Ca2+(aq,s)}$; Moya et al., 2001). $n_{H+(aq,s)}$ was entered to balance charge. E-AIM considers only the most major gas and particle species of each ion (i.e., H_2O(g), HCl(g), HBr(g), HNO_3(g), Cl^-(aq), Br^-(aq), NO_3^-(aq), SO_4^{2-}(aq), HSO_4^-(aq), H^+(aq) in E-AIM1; H_2O(g), HCl(g), HNO_3(g), Cl^-(aq), NO_3^-(aq), SO_4^{2-}(aq), HSO_4^-(aq), H^+(aq), Na^{+*}(aq) and salts of Na^{+*} in E-AIM3). Minor species, such as the associated aqueous forms (H_2SO_4(aq), HCl(aq), HBr(aq), HNO_3(aq)) and the extremely hygroscopic H_2SO_4(g), are not considered within E-AIM.

The variables to be investigated within E-AIM1 are: (1) relative humidity, (2) ambient temperature, (3) the amounts of SO_4^{2-} and halogen and nitric acids (reflecting differences in SO_3 production at the vent, and differences in the magmatic gas composition) and (4) plume dilution. The variables to be investigated within E-AIM3 are: (1) relative humidity and (2) the amount of Na^+ (as a proxy for a wider range of metal ions). Results are independent of the total atmospheric pressure because at fixed temperature RH defines the partial pressure of H_2O ($p_{H2O(g)}$; in atm) and the input composition defines the partial pressure of HCl, HBr and HNO_3 ($p_{HCl(g)}$, $p_{HBr(g)}$ and $p_{HNO3(g)}$; in atm).

We also use a three-parameter model for equilibrium partitioning (e.g., Mather et al., 2003), which considers non-dissociative dissolution of gas (HX) (i.e., Henry's law, $K_{H:X}$; E1A) and the subsequent dissociation into ions (i.e., acidity constants, $K_{A:X}$; E1B). The concentrations of aqueous species are defined by activity (a_i; in mol dm^{-3}), while the concentrations of gaseous species are defined by partial pressure (p_i; in atm). The total concentration of X in the particles is defined by $a_{X(aq)}$ (i.e., $a_{X\text{-}(aq)}$ + $a_{HX(aq)}$) (E2). Literature values of $K_{H:X}$ and $K_{H:A}$ are given in Table 1. The three-parameter model shows that $a_{X(aq)}$ increases with increasing $K_{H:X}$ and $K_{H:A}$, and decreases with increasing $a_{H+(aq)}$. In other words, acidic gas partitioning will decrease as the particles become more acidic.

R1A $HX(g) = HX(aq)$ E1A $$K_{H:X} = \frac{a_{HX(aq)}}{p_{HX(g)}}$$

R1B $HX(aq) = H^+(aq) + X^-(aq)$ E1B $$K_{A:X} = \frac{a_{H+(aq)} a_{X-(aq)}}{a_{HX(aq)}}$$

E2 $$\frac{a_{X(aq)}}{p_{HX(g)}} = K_{H:X}\left(1 + \frac{K_{A:X}}{a_{H+(aq)}}\right)$$

The complexity of the E-AIM model does not allow for a full uncertainty analysis although the uncertainty in the outputs will depend on the uncertainty of the thermodynamic database (Wexler and Clegg, 2002). In general, validation of E-AIM (and other aerosol thermodynamic models) is performed by comparison with field or laboratory measurements over a range of conditions (e.g., Yao et al., 1999; Wexler and Clegg, 2002; Clegg et al., 2008). The uncertainty within the three-parameter model (E2) can be considered within different regimes: (1) $K_{A:X}/a_{H+(aq)} < 1$ and (2) $K_{A:X}/a_{H+(aq)} > 1$.

The uncertainty in E2 is therefore equal to the uncertainty on $K_{H:X}$ or on the product $K_{A:X}K_{H:X}$ (respectively). For strong acids, the product $K_{A:X}K_{H:X}$ is much better constrained than either $K_{A:X}$ and $K_{H:X}$ alone (i.e., there may be 1-2 orders of magnitude uncertainty on $K_{A:X}$ and $K_{H:X}$) because measurement of $K_{A:X}K_{H:X}$ does not require determination of $a_{HX(aq)}$ (only $p_{HX(g)}$, $a_{X-(aq)}$ and $a_{H+(aq)}$). Many more minor halogen species (e.g., $Br_2(aq)$, $Cl_2(aq)$, $I_2(aq)$, BrCl(aq), $Br_2Cl^-(aq)$, $I_3^-(aq)$, $(HF)_n(aq)$) are not considered within the three-parameter model. Calculations of $a_{X(aq)}/p_{HX(g)}$ are therefore lower limits to the true $a_{X(aq)}/p_{HX(g)}$ since only $a_{HX(aq)}$ and $a_{X-(aq)}$ are considered.

3 Results and Discussion

E-AIM1 was used to estimate the equilibrium composition of volcanic aerosol as a function of RH for the standard input composition at 298 K. Results for equilibrium amounts (n_i; in mol m^{-3} of air) and concentrations (c_i; in mol dm^{-3} of solution) of aqueous species are shown in Figure 1. By absolute amount, the most important change with increasing RH is increasing $n_{H2O(aq)}$, resulting in dilution of the aqueous phase and an increase in particle size. The responses of different chemical equilibria to dilution result in complex compositional changes. H^+ and HSO_4^- are the most abundant ions at low RH and exist in approximately equal amounts. Dilution of the aqueous phase promotes the dissociation of HSO_4^- into SO_4^{2-} and H^+ although the net effect is decreasing $c_{H+(aq)}$ (and thus increasing pH) with increasing RH.

The extent of HCl partitioning, which is represented by $n_{Cl-(aq)}$, is quantitatively minor (<1% of initial $n_{HCl(g)}$) below 80% RH but near-complete (>95%) above 95% RH (Figure 1). The increase in HCl partitioning above 80% RH (which we denote RH_{crit}) reflects $Cl^-(aq)$ becoming the most abundant anion (i.e., $n_{Cl-(aq)} > n_{SO42-(aq)} + n_{HSO4-(aq)}$). The significance is that changes in $n_{Cl-(aq)}$ may now influence $n_{H2O(aq)}$, or equivalently, that particle hygroscopicity is controlled by HCl rather than H_2SO_4. In this regime, $n_{Cl-(aq)}$ and $n_{H2O(aq)}$ both increase with RH, allowing a large change in $n_{Cl-(aq)}$ for only a small change in $c_{Cl-(aq)}$. Eventually, the increase in $n_{H2O(aq)}$ exceeds the increase in $n_{Cl-(aq)}$ as the supply of HCl(g) is exhausted, resulting in decreasing $c_{Cl-(aq)}$. The similarity between trends in HCl and HNO_3 partitioning (i.e., $n_{NO3-(aq)}$) above RH_{crit} reflects the influence of HCl on $n_{H2O(aq)}$, while the differences

178 at low RH reflect greater $K_{H:X}$ for HNO_3 than HCl. HBr partitioning (i.e., $n_{Br\text{-}(aq)}$) occurs more readily
179 than HCl or HNO_3 partitioning, being minor below 60% RH and near-complete above 85% RH. Thus,
180 at low RH, $n_{Br\text{-}(aq)}/n_{Cl\text{-}(aq)}$ is greater than initial $n_{HBr(g)}/n_{HCl(g)}$ (and, equivalently, initial $p_{HBr(g)}/ p_{HCl(g)}$),
181 implying a relative enrichment of the particle phase with Br. These differences reflect the greater
182 acidity of HBr than either HCl or HNO_3 (Table 1), which allows for HBr partitioning into the highly
183 acidic particle phase present below RH_{crit}. The increase in $n_{H2O(aq)}$ at RH_{crit} has little effect on $n_{Br\text{-}(aq)}$,
184 which is already close to its maximum value (defined by initial $n_{HBr(g)}$).

185 E-AIM1 calculations were also made at 283 K and 313 K (Figure 1). The 283 K - 313 K temperature
186 range was chosen because it is centred on 298 K (allowing comparison of results between E-AIM1
187 and E-AIM3) and spans the range of ambient temperatures recorded at Masaya (e.g., Mather et al.,
188 2003, 2006). Below RH_{crit}, $n_{Cl\text{-}(aq)}$, $n_{Br\text{-}(aq)}$ and $n_{NO3\text{-}(aq)}$ decrease by a factor of 10 between 283 K and
189 313 K, with the direction of the trend being consistent with the exothermic nature of the process (i.e.,
190 the sum of R1A and R1B). $n_{Cl\text{-}(aq)}$ and $n_{NO3\text{-}(aq)}$ are even more sensitive to temperature around RH_{crit},
191 because RH_{crit} itself increases with temperature.

192 To investigate the different influences of (input) SO_4^{2-} and HCl on acidic gas partitioning, E-AIM1
193 calculations were made for the standard input composition at 298 K, with initial $n_{SO42\text{-}(aq,s)} = 0$, 0.2, 2,
194 20 μmol m^{-3} (Figure 2A), and separately, with initial $n_{HCl(g)}$=0, 40, 400, 4000 μmol m^{-3} (Figure 2B).
195 For simplicity, only $n_{Cl\text{-}(aq)}$ and $n_{H2O(aq)}$ are shown in each Figure. Figure 2A (i.e., variable SO_4^{2-})
196 shows that below RH_{crit}, both $n_{H2O(aq)}$ and $n_{Cl\text{-}(aq)}$ are proportional to SO_4^{2-}, hence RH_{crit} is independent
197 of SO_4^{2-}. Above RH_{crit}, $n_{Cl\text{-}(aq)}$ is independent of SO_4^{2-}, consistent with particle hygroscopicity being
198 controlled by HCl rather than H_2SO_4. Figure 2B (i.e., variable HCl) shows that decreasing HCl results
199 in increasing RH_{crit}, since a higher RH must be reached before Cl^-(aq) becomes the most abundant
200 anion. Consistent with our interpretation, $n_{H2O(aq)}$ increases with HCl above RH_{crit}, but is independent
201 of HCl below RH_{crit}. An additional calculation was made for the standard input composition with
202 initial $n_{HCl(g)} = n_{HBr(g)} = n_{HNO3(g)} = 0$ μmol m^{-3}. Here, $n_{H2O(aq)}$ was similar to $n_{H2O(aq)}$ calculated for the

standard input composition with initial $n_{HCl(g)}$=0 μmol m^{-3}, indicating that neither HBr nor HNO_3 have a significant influence on $n_{H2O(aq)}$.

Plume dilution has the effect of decreasing SO_4^{2-} and HCl together. To investigate this influence on acidic gas partitioning, E-AIM1 calculations were made with D/D_0 = 0.1, 1, 10, 100 (where D_0 is the dilution at the crater rim) and the standard input composition at 298 K (Figure 2C). Input concentrations are proportional to D^{-1}, except $p_{H2O(aq)}$, which is fixed by RH. We assume that the aerosol volume within the background atmosphere is negligible. Below RH_{crit}, $n_{H2O(aq)}$ is proportional to SO_4^{2-} (Figure 2A) and hence proportional to D^{-1}. In contrast, $n_{Cl-(aq)}$ is proportional to D^{-2}, because both $n_{H2O(aq)}$ and $n_{HX(g)}$ are proportional to D^{-1}. Thus, a 10-fold plume dilution (D/D_0=10) results in a 10-fold decrease in $n_{H2O(aq)}$ and a 10-fold decrease in $n_{HCl(g)}$, resulting in a 100-fold decrease in $n_{Cl-(aq)}$. These factors affect RH_{crit} so $n_{Cl-(aq)}$ is highly sensitive to D around RH_{crit}. A limitation of the model is that as D/D_0 increases, SO_4^{2-} tends to zero, rather than the true atmospheric background, resulting in an underestimate of partitioning at high D/D_0.

E-AIM3 was used to estimate the equilibrium composition of volcanic aerosol as a function of RH and equivalent Na^{*+} ($n_{Na^{*+}(aq,s)}$, i.e., the total amount of Na^{*+} in the aqueous and solid phases) for the standard input composition at 298 K. Calculations were made by introducing equal amounts of Na^{*+} and Cl, simulating the addition of NaCl to acidic sulphate particles (e.g., Óskarsson, 1980). Results for equilibrium amounts of aqueous species and salts are shown in Figure 3. Equilibrium amounts of Na-sulphate salts ($NaHSO_4.H_2O$, $Na_3H(SO_4)_2$, Na_2SO_4) are summed and shown as "other Na*(s)" on Figure 3. The system shows complex behaviour because of salt formation. At low RH (e.g., 50%), increasing $n_{Na^{*+}(aq,s)}$ results in decreasing $n_{H2O(aq)}$, $n_{H+(aq)}$, $n_{Cl-(aq)}$ and $n_{NO3-(aq)}$. Further increases in $n_{Na^{*+}(aq,s)}$ result in the crystallisation of less hygroscopic Na-sulphate salts rather than aqueous solutions. The net result is that HCl partitioning decreases with increasing $n_{Na^{*+}(aq,s)}$ due to a decrease in the water content of the particle, and only increases when all SO_4^{2-} has been associated with Na^{*+} and NaCl forms (i.e., the stable assemblage is Na_2SO_4 + NaCl). HNO_3 partitioning does not increase with increasing $n_{Na^{*+}(aq,s)}$ because no Na-nitrates are formed (although these are considered within E-

AIM3). In contrast, at high RH (e.g., 75%), increasing $n_{Na^*+(aq,s)}$ results in increasing $n_{H2O(aq)}$, $n_{Cl\text{-}(aq)}$, $n_{NO3\text{-}(aq)}$ and decreasing $n_{H+(aq)}$. No salts are formed under these conditions as RH exceeds the deliquescence RH (DRH) of all salts formed at lower RH (i.e., Na-sulphates, NaCl). The decreasing $n_{H+(aq)}$ reflects the volatilisation of HCl, shown by the initially greater increase of $n_{Na+(aq)}$ than $n_{Cl\text{-}(aq)}$ with increasing $n_{Na^*+(aq,s)}$. We suggest that HBr (not considered within E-AIM3) and other acidic gases will show similar trends to HCl and HNO_3.

Figure 4 shows calculations for HCl, HBr and HNO_3 partitioning, expressed as $a_{X(aq)}/p_{HX(g)}$, from the three-parameter model (E2). Also shown are calculations for HCl, HBr and HNO_3 partitioning from E-AIM1. A good agreement is found between results from the three-parameter model and E-AIM1, and the non-consideration of HBr(aq) and HCl(aq) within E-AIM1 appears justified in the case of highly acidic sulphate particles. However, HNO_3 partitioning into acidic sulphate particles may be underestimated within E-AIM1 because HNO_3(aq) is not considered (only NO_3^-(aq)). In the three-parameter model, $a_{X(aq)}/p_{HX(g)}$ for HNO_3 stabilises above $K_{A:NO3}$ (corresponding to below ~60% RH) because HNO_3(aq) is present in greater abundance than NO_3^-(aq). We may speculate that HNO_3(aq) was not included within E-AIM1 because HNO_3(aq) is unstable in other less acidic atmospheric aerosols. Hence, while the uncertainties on $a_{X(aq)}/p_{HX(g)}$ within E-AIM1 for HCl and HBr are small and only relate to the uncertainties on the product $K_{A:X}K_{H:X}$, the uncertainties on $a_{X(aq)}/p_{HX(g)}$ for HNO_3 (at low RH) are potentially much larger. However, since NO_3 is a minor component of the particle phase in volcanic emissions (e.g., Table 2), underestimation of $a_{X(aq)}/p_{HX(g)}$ for HNO_3 is unlikely to compromise E-AIM results for other species.

HBr and HI partitioning (Figure 4) are predicted to be similar in terms of $a_{X(aq)}/p_{HX(g)}$ due to the similarity in the product $K_{H:X}K_{A:X}$ (Table 1). This result suggests that an estimate of $n_{I\text{-}(aq)}$ can be made by substituting HI for HBr within the E-AIM1 model and calculating $n_{I\text{-}(aq)}$ as $n_{Br\text{-}(aq)}$. This approximation is justified because the differences in the activity coefficients (γ) of Br^-(aq) and I^-(aq) are small over a wide range of conditions (e.g., Hamer and Wu, 1972; Brimblecombe and Clegg, 1988) and because HBr has no influence on $n_{H2O(aq)}$ (Figure 2B). Within the three-parameter model, HF partitioning is predicted to be independent of a_{H+} over a wide range of RH (<99%) because

HF(aq) is more abundant than F^-(aq) in acidic particles. $n_{HF(aq)}$ can be estimated from E1A, substituting $a_{HF(aq)} = \gamma n_{HF(aq)}/V$, where V is the aerosol volume, and $p_{HF(g)} = \beta(n_{HF(g):0} - n_{HF(aq)})$, where $n_{HF(g):0}$ is initial $n_{HF(g)}$ (Table 2) and β is the conversion factor between 1 atm and 1 mol m^{-3} at 298 K. This approximation (E3) assumes that HF partitioning influences neither V nor the activity of other components of the particle phase, and is justified if $n_{HF(aq)}$ remains a minor component of the particle phase. HCl, HBr and HI have large γ at low RH (> 100), while HF has a small γ at low RH (e.g., < 1), which would promote uptake according to E3.

E3 $$n_{HF(aq)} = \frac{(\beta K_{H:F} V)}{(\gamma + \beta K_{H:F} V)} n_{HF(g):0}$$

Figure 4 shows estimates for HI partitioning (assuming $\gamma_{HI} = \gamma_{HBr}$) and HF partitioning (assuming γ_{HF}=1) into volcanic aerosol as a function of RH for the standard input composition at 298 K. HCl, HBr and HNO_3 partitioning are shown for comparison. At low RH, the extent of HF partitioning is greater than that of the other halogens, which have small $K_{H:X}$ but large $K_{A:X}$. Increasing RH has little influence on HF partitioning until RH_{crit} is reached, when V increases significantly, causing an increase in $n_{HF(aq)}$. Within the approximation, HI and HBr partitioning are proportional over all RH. This simply reflects the constancy of the ratio $a_{X(aq)}/p_{HX(g)}$ (E2) with fixed $a_{H+(aq)}$. These results indicate that at low RH, the particle phase is enriched in F, and to a lesser extent Br and I, relative to the gas-phase composition (Table 2).

3.3 Implications for volcanology and environmental geochemistry

In summary, the equilibrium partitioning of acidic gases into acidic sulphate particles is maximised at high RH and low temperature, in near-source (i.e., less dilute) plumes with high SO_4^{2-}/SO_2 The addition of NaCl enhances acidic gas partitioning at high RH, but diminishes acidic gas partitioning at low RH due to the formation of Na-sulphate salts.

HCl partitioning is predicted to exceed 1% of total HCl at ~80% RH and be near-complete (>95%) above 95%, indicating that spectroscopic or electrochemical measurements of magmatic gas-phase

280 SO_2/HCl from the crater-rim are robust below 80% RH. At higher RH, HCl partitioning may result in
281 erroneously high measured SO_2/HCl ratios. This effect is intensified by the fact that high RH is often
282 associated with lower temperatures (e.g., at night-time). Burton et al., (2001) reported an apparent loss
283 of 38% HCl to the particle phase, by comparison of SO_2/HCl ratios in the day-time (302 K, 42% RH,
284 using solar occultation FTIR spectroscopy) and the night-time (292 K, 93% RH, using lunar
285 occultation FTIR spectroscopy). While their model for HCl partitioning was incomplete (i.e., H_2SO_4
286 was not considered), our modelling results support their conclusions that the difference in SO_2/HCl
287 may be explained in terms of HCl partitioning. HNO_3, HBr and HI are not measured routinely in the
288 field, although partitioning is also predicted to be significant above ~80% RH. These results should be
289 taken into account when planning measurement strategies or when interpreting data from continuous
290 gas monitoring.

291 Over a wide range of atmospheric conditions acidic gas partitioning has negligible influence on gas-
292 phase concentrations, e.g., $p_{HCl(g)}$, $p_{HBr(g)}$, $p_{HI(g)}$, $p_{HNO3(g)}$ and $p_{HF(g)}$. However, a small change in
293 temperature and/or RH may significantly affect the amounts of particle forms of acidic gases, e.g., $n_{Cl\text{-}(aq)}$,
294 $n_{Br\text{-}(aq)}$, $n_{I\text{-}(aq)}$, $n_{NO3\text{-}(aq)}$ and $n_{HF(aq)}$. This would result in increased acidic gas partitioning in the night-
295 time, when temperatures are typically lower and RH higher, consistent with clear diurnal trends in $n_{Cl\text{-}(aq)}$
296 at Masaya (Mather et al., 2003). Furthermore, since particle size also increases at high RH due to
297 water uptake (e.g., Figure 1), the rate of acidic gas deposition would be expected to increase during
298 the night-time. Equally, as RH is high during the wet season (April - October), acidic gas deposition
299 may be enhanced at certain times of the year, which may impact negatively on seasonal crop growth
300 (e.g., Delmelle et al., 2002). This seasonal influence is potentially shown by measurements of $n_{Cl\text{-}(aq,s)}$
301 at Masaya, which were lower than background in March/April (in 2007, 2009 and 2010; Martin et al.,
302 2011), and higher than background in December (2001; Mather et al., 2003). Our results indicate that
303 the relative rates of deposition of HF, HCl, HBr, HI and HNO_3 (in particle form) may differ from the
304 relative abundances of the gases, due to increasing partitioning of HF, and to a lesser extent HBr and
305 HI, relative to HCl at low RH. In contrast, at high RH the relative rates of deposition will more

306 closely mimic the relative abundances of the gases. This is exploited by studies using rainwater
307 chemistry as a direct proxy for magmatic gas composition (e.g., Aiuppa et al., 2006).

308 Within the internal mixtures considered in this study, particles are dominated by SO_4^{2-} or HSO_4^-
309 below 80% RH and by Cl^- above 80% RH. HCl partitioning below 80% RH is inhibited due to the
310 acidity of the aerosol. Alternatively, particles in different size fractions may be compositionally
311 distinct (i.e., an external mixture), with only particles in the same size fraction forming an internal
312 mixture (e.g., Mather et al., 2004; Martin et al., 2011). This may enhance acidic gas partitioning as
313 acidic gases interact preferentially with the less acidic particles within the size distribution. While
314 halogen and nitric acids do not react directly with water to form Cl^--rich aqueous particles (except
315 above 80% RH, although even this may be hindered by the slow rate of homogenous nucleation), Cl^--
316 rich particles may be stable at any RH by salt formation. Requirements for a "stable" size distribution
317 with enhanced acidic gas partitioning (i.e., greater overall Cl^-/SO_4^{2-} than predicted for a fully internal
318 mixture) are therefore a size separation of H^+ and Cl^-, and a size association of Cl^- and metal ions.
319 These conditions appear to be met in the case of Masaya, where particle size measurements indicate a
320 fine mode of Na^+-K^+-H^+-SO_4^{2-} and a coarse mode of Mg^{2+}-Ca^{2+}-Cl^--F^- (e.g., Mather et al., 2003;
321 Martin et al., 2011), with overall $n_{Cl\text{-}(aq,s)}/n_{SO42\text{-}(aq,s)}$ = 0.2 (Table 2). In contrast, while particle size
322 measurements at Villarrica volcano (Chile) (Mather et al., 2004) indicate a size association between
323 H^+, SO_4^{2-} and Cl^-, overall $n_{Cl\text{-}(aq,s)}/n_{SO42\text{-}(aq,s)}$ (= 0.006) is much lower than at Masaya.

324 Our results also have implications for physical and chemical processing in volcanic plumes.
325 Entrainment of air into the plume and dilution results in decreased aerosol volume (assuming that the
326 background aerosol volume is negligible) and decreased gas concentrations, which would promote
327 evaporation of halogen and nitric acids from the particles. Further complexity is introduced by the
328 dependence of partitioning on temperature and relative humidity. These factors may inhibit or
329 promote heterogeneous chemistry under certain conditions. In any case, it is likely that the
330 partitioning of halogen and nitric acids may have a strong spatial and temporal variation. Our results
331 are important because they establish the intrinsic thermodynamic influences on plume evolution.
332 Furthermore, as only a few processes are considered, the results offer an insight into plume evolution

in the absence of the more complex chemistry considered within ambient temperature model studies (e.g., Roberts et al., 2009; von Glasow, 2010), or suggested from field measurements (e.g., SO_2 oxidation at ambient temperature; Oppenheimer et al., 2010).

4 Conclusions

The uptake of halogen and nitric acids into acidic sulphate particles is a fundamental process with wide implications in volcanology and the environmental geochemistry of volcanic emissions.

Using the thermodynamic Aerosol Inorganics Model (E-AIM; Wexler and Clegg, 2002) for HCl, HBr and HNO_3, combined with a simple three-parameter model for HF and HI (e.g., Mather et al., 2003), we show that the equilibrium partitioning of halogen and nitric acids into acidic sulphate particles is maximised at high relative humidity and low temperature, in near-source (i.e., less dilute) volcanic plumes with high SO_4^{2-}/SO_2. The addition of NaCl enhances acidic gas partitioning at high RH, but diminishes acidic gas partitioning at low RH due to a decrease in the water content of the particles and the formation of Na-sulphate salts. We predict that acidic gas partitioning into acidic sulphate particles is quantitatively significant (>1%) only in cool humid conditions (e.g., > 80% RH at 298 K), adding confidence to spectroscopic and/or electrochemical determinations of gas ratios (e.g., SO_2/HCl, HCl/HF) for volcano monitoring. Over a wider range of atmospheric conditions, acidic gas partitioning remains environmentally important because of significant changes in the amounts of particle forms of acidic gases, e.g., HF(aq), Cl^-(aq), Br^-(aq), I^-(aq) and NO_3^-(aq). This influence may result in increased rates of acidic gas deposition during the times of increased RH, such as the night-time and during the wet season.

Despite the inherent limitations of the equilibrium assumption (i.e., is equilibrium attained over an appropriate timescale?) and parametric modelling (i.e., are variables independent?), our results are important because they establish the intrinsic thermodynamic influences on plume evolution. These influences are complementary to the kinetic influences (i.e., chemical reactivity, dispersion) considered within more complex models of ambient temperature plume evolution.

5 Acknowledgements

RSM thanks Christ's College, University of Cambridge for Junior Research Fellowship.

6 References

Aiuppa A., Bellomo S., Brusca L., D'Alessandro, Di Paola R., and Longo M., 2006. Major-in bulk deposition around an active volcano (Mt. Etna, Italy). Bulletin of Volcanology 68, 255-265.

Allen A.G., Mather T.A., McGonigle A.J.S., Aiuppa A., Delmelle P., Davison B., Bobrowski N., Oppenheimer C., Pyle D.M., and Inguaggiato S., 2006. Sources, size distribution and downwind grounding of aerosols from Mt. Etna. Journal of Geophysical Research 111, D10302.

Ammann M., and Burtscher H., 1990. Characterisation of ultrafine particles in Mt. Etna emissions. Bulletin of Volcanology 52, 577-583.

Ammann M., Hauert R., Burtscher H., Siegmann H.-C., 1993. Photoelectric charging of ultrafine volcanic aerosols: detection of Cu(I) as a tracer of chloride in magmatic gases. Journal of Geophysical Research 98, 551-556.

Bellomo S., Aiuppa A., D'Alessandro W., and Parello F., 2007. Environmental impact of magmatic fluorine emission in the Mt. Etna area. Journal of Volcanology and Geothermal Research 165, 87–101.

Bobrowski N., von Glasow R., Aiuppa A., Inguaggiato S., Louban I., Ibrahim O.W., and Platt U., 2007. Reactive halogen chemistry in volcanic plumes. Journal of Geophysical Research 112, D06311.

Boichu M., Oppenheimer C., Roberts T.J., Tsanev V., and Kyle P.R., 2011. On bromine, nitrogen oxides and ozone depletion in the tropospheric plume of Erebus volcano (Antarctica). Atmospheric Environment 45(23), 3856-3866.

379 Brimblecombe, P., and Clegg, S.L., 1988. The solubility and behaviour of acid gases in the marine
380 aerosol. Journal of Atmospheric Chemistry 7, 1-18.

381 Burton M., Oppenheimer C., Horrocks L.A., Francis P.W., 2001. Diurnal changes in volcanic plume
382 chemistry observed by lunar and solar occultation spectroscopy. Geophysical Research Letters 28(5),
383 843-846.

384 Carslaw K.S., Clegg S.L., and Brimblecombe P., 1995. A thermodynamic model of the system HCl -
385 HNO_3 - H_2SO_4 - H_2O, including solubilities of HBr, from <200 K to 328 K. Journal of Physical
386 Chemistry 99, 11557-11574.

387 Clegg S.L., Brimblecombe P., and Wexler A.S., 1998. A thermodynamic model of the system H^+ -
388 NH_4^+ - Na^+ - SO_4^{2-} - NO_3^- - Cl^- - H_2O at 298.15 K. Journal of Physical Chemistry A 102, 2155-2171.

389 Clegg S.L., Kleeman M.J., Griffin R.J., and Seinfeld J.H., 2008. Effects of uncertainties in the
390 thermodynamic properties of aerosol components in an air quality model – Part 1: Treatment of
391 inorganic electrolytes and organic compounds in the condensed phase. Atmospheric Chemistry and
392 Physics 8, 1057-1085.

393 Delmelle P., Stix J., Baxter P., Garcia-Alvarez J., Barquero J., 2002. Atmospheric dispersion,
394 environmental effects and potential health hazard associated with the low altitude gas plume of
395 Masaya volcano, Nicaragua. Bulletin of Volcanology 64, 423-434.

396 Duffell H.J., Oppenheimer C., Pyle D.M, Galle B., McGonigle A.J.S., and Burton M.R., 2003.
397 Changes in gas composition prior to a minor explosive eruption at Masaya volcano, Nicaragua.
398 Journal of Volcanology and Geothermal Research 126, 327-339.

399 Fountoukis C., and Nenes A., 2007. ISORROPIA II: A Computationally Efficient Aerosol
400 Thermodynamic Equilibrium Model for K^+, Ca^{2+}, Mg^{2+}, NH_4^+, Na^+, SO_4^{2-}, NO_3^-, Cl^-, H_2O Aerosols.
401 Atmospheric Chemistry and Physics 7, 4639–4659.

402 Gerlach T.M., 2004. Volcanic sources of tropospheric ozone-depleting trace gases. Geochemistry
403 Geophysics Geosystems 5, Q09007.

404 Greenwood N.N., and Earnshaw A., 1997. Chemistry of the elements. Elsevier, Oxford, UK.1342p

405 Hamer W.J., and Wu Y-C, 1972. Osmotic coefficients and mean activity coefficients of uni-univalent
406 electrolytes in water at 25 °C. Journal of Physical Chemistry Reference Data 1(4), 1047-1100.

407 Horrocks L., Burton M., Francis P., and Oppenheimer C., 1999. Stable Gas Plume Composition
408 Measured by OP-FTIR Spectroscopy at Masaya Volcano, Nicaragua, 1998-1999. Geophysical
409 Research Letters 26, 3497-3500.

410 Huebert B., Vitousek P., Sutton J., Elias T., Heath J., Coeppicus S., Howell S., and Blomquist B.,
411 1999. Volcano fixes nitrogen into plant-available forms. Biogeochemistry 47(1), 111-118.

412 Martin R.S., Mather T.A., and Pyle D.M., 2006. High-temperature mixtures of magmatic and
413 atmospheric gases. Geochemistry Geophysics Geosystems 7, Q04006.

414 Martin R.S., Mather T.A., Pyle D.M., Power M., Allen A.G., Aiuppa A., Horwell C.J., and Ward
415 E.P.W., 2008. Composition-resolved size distributions of volcanic aerosols in the Mt. Etna plumes.
416 Journal of Geophysical Research 113, D17211.

417 Martin R.S., Sawyer G.M., Spampinato L., Salerno G.G., Ramirez C., Ilyinskaya I., Witt M.L.I.,
418 Mather T.A., Watson I.M., Phillips J.C., and Oppenheimer C., 2010. A total volatile inventory for
419 Masaya volcano, Nicaragua. Journal of Geophysical Research 115, B09215.

420 Martin R.S., Ilyinskaya E., Sawyer G.M., Tsanev V.I., Oppenheimer C., 2011. A re-assessment of
421 aerosol size distributions from Masaya volcano (Nicaragua). Atmospheric Environment 45(3), 547-
422 560.

423 Mather T.A., Allen A.G., Oppenheimer C., Pyle D.M., McGonigle A.J.S., 2003. Size-resolved
424 characterisation of soluble ions in the particles in the tropospheric plume of Masaya volcano,
425 Nicaragua: Origins and plume processing. Journal of Atmospheric Chemistry 46, 207-237.

426 Mather T.A., Allen A.G., Davison B.M., Pyle D.M., Oppenheimer C., and McGonigle A.J.S., 2004.
427 Nitric Acid from Volcanoes. Earth and Planetary Science Letters 218, 17-30.

428 Mather T.A., Pyle D.M., Tsanev V.I., McGonigle A.J.S., Oppenheimer C., and Allen A. G., 2006a. A
429 reassessment of current volcanic emissions from the Central American arc with specific examples
430 from Nicaragua. Journal of Volcanology and Geothermal Research 149, 297-311.

431 Moune S., Gauthier P.-J., and Delmelle P., 2010. Trace elements in the particulate phase of the plume
432 of Masaya Volcano, Nicaragua. Journal of Volcanology and Geothermal Research 193, 232-244.

433 Moya M., Ansari A.S., and Pandis S.N., 2001. Partitioning of nitrate and ammonium between the gas
434 and particulate phases during the 1997 IMADA-AVER study in Mexico City. Atmospheric
435 Environment 35(10), 1791-1804.

436 Oppenheimer C., Tsanev V.I., Braban C.F., Cox R.A., Adams J.W., Aiuppa A., Bobrowski N.,
437 Delmelle P., Barclay J., and McGonigle A.J.S., 2006. BrO formation in volcanic plumes. Geochimica
438 et Cosmochimica Acta 70, 2935-2941.

439 Oppenheimer C., Kyle P., Eisele F., Crawford J., Huey G., Tanner D., Saewung K., Mauldin L., Blake
440 D., Beyersdorf A., Buhr M., Davis D., 2010. Atmospheric chemistry of an Antarctic volcanic plume.
441 Journal of Geophysical Research 115: D04303.

442 Óskarsson, N., 1980. The interaction between volcanic gases and tephra: Fluorine adhering to tephra
443 of the 1970 Hekla eruption. Journal of Volcanology and Geothermal Research 8(2-4), 251-266.

444 Pyle D.M., and Mather T.A., 2009. Halogens in igneous processes and their fluxes to the atmosphere
445 and oceans from volcanic activity: A review. Chemical Geology 263 (1-4), 110-121.

446 Roberts T.J., Braban C.F., Martin R.S., Oppenheimer C., Adams J.W., Cox R.A., Jones R.L., and
447 Griffiths P.T., 2009. Modelling reactive halogen formation and ozone depletion in volcanic plumes.
448 Chemical Geology 263, 110-121.

449 Symonds R.B., Reed M.H., and Rose W.I., 1992. Origin, speciation and fluxes of trace-element gases
450 at Augustine volcano, Alaska: Insights into magma degassing and fumarolic processes. Geochimica et
451 Cosmochimica Acta 56, 633-657.

452 Symonds R.B., and Reed M.H., 1993. Calculation of multicomponent chemical equilibria in gas-
453 solid-liquid systems: calculation methods, thermochemical data and applications to studies of high-
454 temperature volcanic gases with examples from Mount St Helens, American Journal of Science 293,
455 758-864.

456 Toutain J.P., Quisefit J.P., Briole P., Aloupogiannis P., Blanc P., and Robaye G., 1995. Mineralogy
457 And Chemistry Of Solid Aerosols Emitted From Mount Etna. Geochemical Journal 29, 163-173.

458 von Glasow, R. 2010. Atmospheric chemistry in volcanic plumes. Proceedings of the National
459 Academy of Sciences of the United States of America 107, 6594-6599.

460 Watt S.F.L, Pyle D.M., Mather T.A., Day J.A., and Aiuppa A., 2007. The use of tree-rings and foliage
461 as an archive of volcanogenic cation deposition. Environmental Pollution 148, 48–61.

462 Wexler A.S., and Clegg S.L., 2002. Atmospheric aerosol models for systems including the ions H^+,
463 NH_4^+, Na^+, SO_4^{2-}, NO_3^-, Cl^-, Br^-, and H_2O. Journal of Geophysical Research 107, 4207.

464 Wexler A.S., and Seinfeld J.H., 1992. Analysis of aerosol ammonium nitrate: Departures from
465 equilibrium during SCAQS. Atmospheric Environment A 26(4), 579-591.

466 Yao Y., Massucci M., Clegg S.L., Brimblecombe P., 1999. Equilibrium Water Partial Pressures and
467 Salt Solubilities in Aqueous NH_4HSO_4 to Low Temperatures. Journal of Physical Chemistry A 103,
468 3678-3686.

469

TABLE 1

Henry's law ($K_{H:X}$) and acidity ($K_{A:X}$) constants for the halogen and nitric acids. K_H was calculated from values of $K_{H:X}K_{A:X}$ (Brimblecombe and Clegg, 1988) and $K_{A:X}$ (Greenwood and Earnshaw, 1997).

Species	$K_H^{(1)}$ (mol dm^{-3} atm^{-1})	$K_A^{(2)}$ (mol dm^{-3})	$K_{H:X}K_{A:X}^{(1)}$ (mol^2 dm^{-6} atm^{-1})
HNO_3	9.6×10^4	2.5×10^1	2.5×10^6
HF	9.6×10^3	1×10^{-3}	9.6×10^0
HCl	2.0×10^{-1}	1×10^7	2.0×10^6
HBr	1.3×10^0	1×10^9	1.3×10^9
HI	2.5×10^{-2}	1×10^{11}	2.5×10^9

TABLE 2

Gas and aerosol composition for Masaya volcano (Nicaragua) (Martin et al., 2010). The standard composition for E-AIM was defined by the values in bold (i.e., HNO_3, HCl, HBr, SO_4^{2-} and Na*+)

Gas phase	Concentration (μmol m^{-3})	Particle phase	Concentration (μmol m^{-3})
$n_{SO2(g)}$	400	$\boldsymbol{n_{SO42-(aq,s)}}$	**2**
$\boldsymbol{n_{HNO3(g)}}$	**0.2**	$n_{NO3-(aq,s)}$	0.03
$n_{HF(g)}$	60	$n_{F-(aq,s)}$	0.1
$\boldsymbol{n_{HCl(g)}}$	**400**	$n_{Cl-(aq,s)}$	0.4
$\boldsymbol{n_{HBr(g)}}$	**0.1**	$n_{Na+(aq,s)}$	2
$n_{HI(g)}$	0.005	$\boldsymbol{n_{Na*+(aq,s)}}$	**3**

FIGURE 1

E-AIM1 results for the equilibrium amounts of selected aqueous species (n_i; in mol m^{-3} of air) for the standard input composition at 283 K, 298 K and 313 K. Also shown are the equilibrium concentrations (c_i; in mol dm^{-3} of solution) of all aqueous species considered at 298 K. RH_{crit} is indicate by a vertical dashed line.

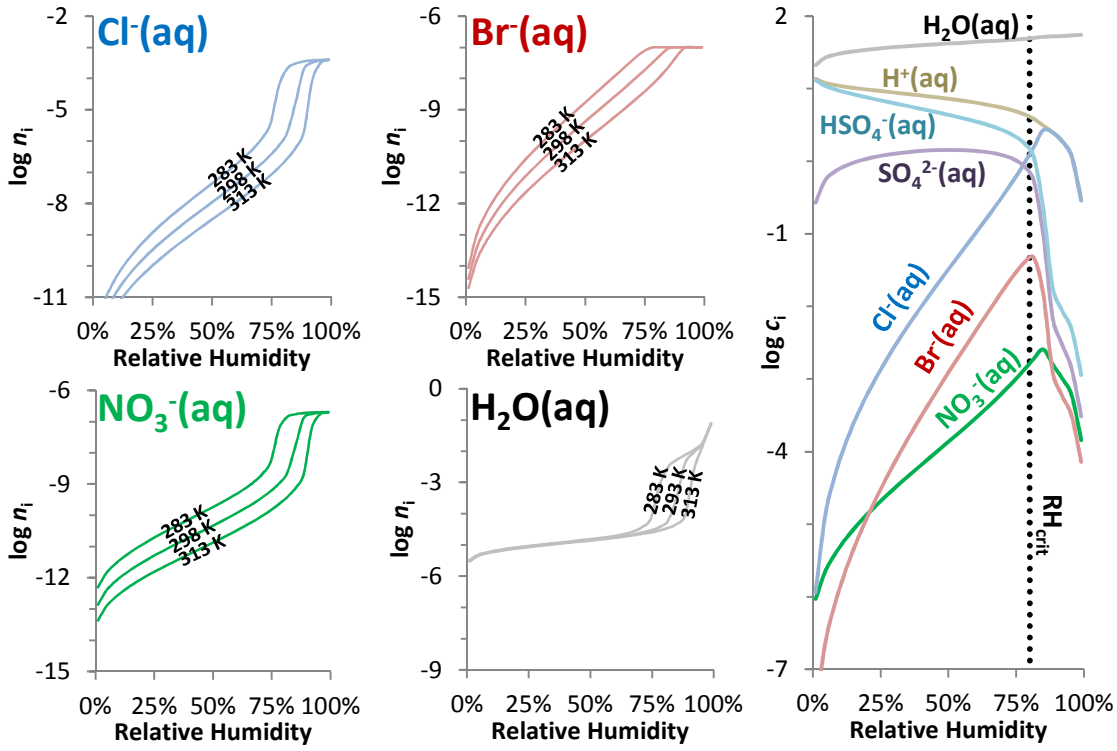

FIGURE 2A

E-AIM1 results for $n_{Cl\text{-}(aq)}$ and $n_{H2O(aq)}$ (mol m^{-3}) for the standard input composition with initial $n_{SO42\text{-}(aq,s)}$ = 0, 0.2, 2, 20 µmol m^{-3} at 298 K.

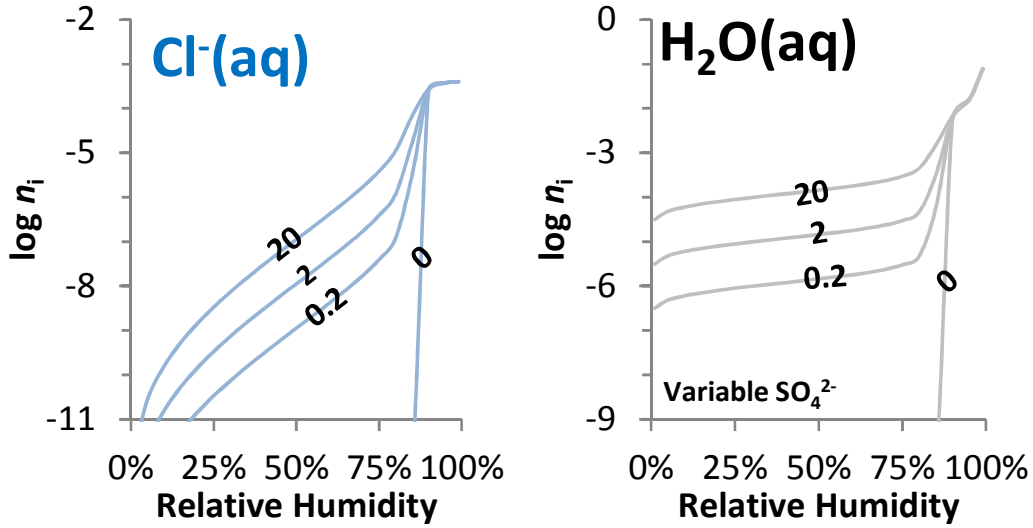

FIGURE 2B

E-AIM1 results for $n_{Cl\text{-}(aq)}$ and $n_{H2O(aq)}$ (mol m^{-3}) for the standard input composition with initial $n_{HCl(g)}$=0, 40, 400, 4000 µmol m^{-3} at 298 K. An additional calculation was made with initial $n_{HCl(g)}$ = $n_{HBr(g)}$ = $n_{HNO3(g)}$ = 0 µmol m^{-3} at 298 K (i.e., SO_4^{2-} only).

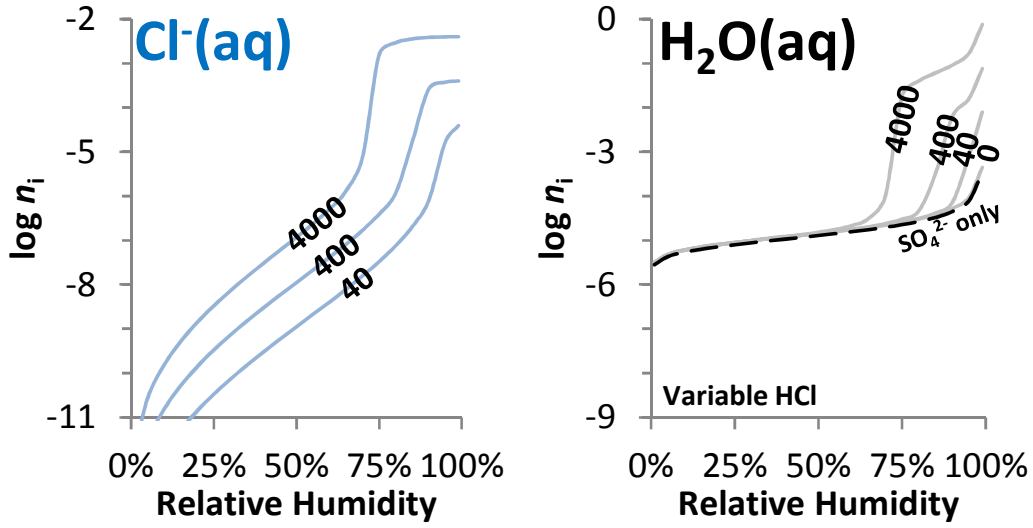

FIGURE 2C

E-AIM1 results for $n_{Cl\text{-}(aq)}$ and $n_{H2O(aq)}$ (mol m^{-3}) for the standard input composition with dilutions (D/D_0) of 0.1, 1 and 10 at 298 K.

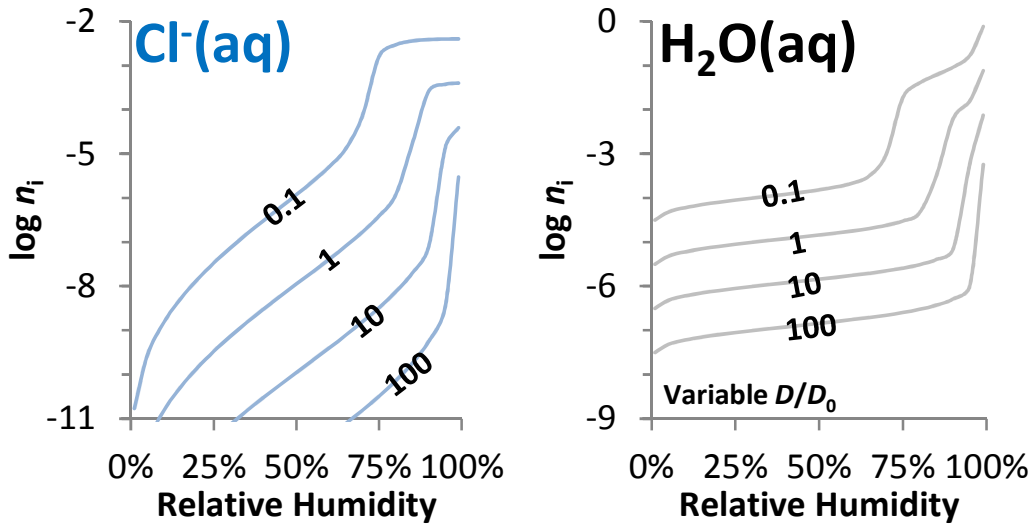

FIGURE 3

E-AIM3 results for equilibrium amounts various species (n_i; in mol m^{-3} of air) for the standard input composition with varying $n_{Na^{*+}(aq,s)}$ at 50% RH and 75% RH, at 298 K.

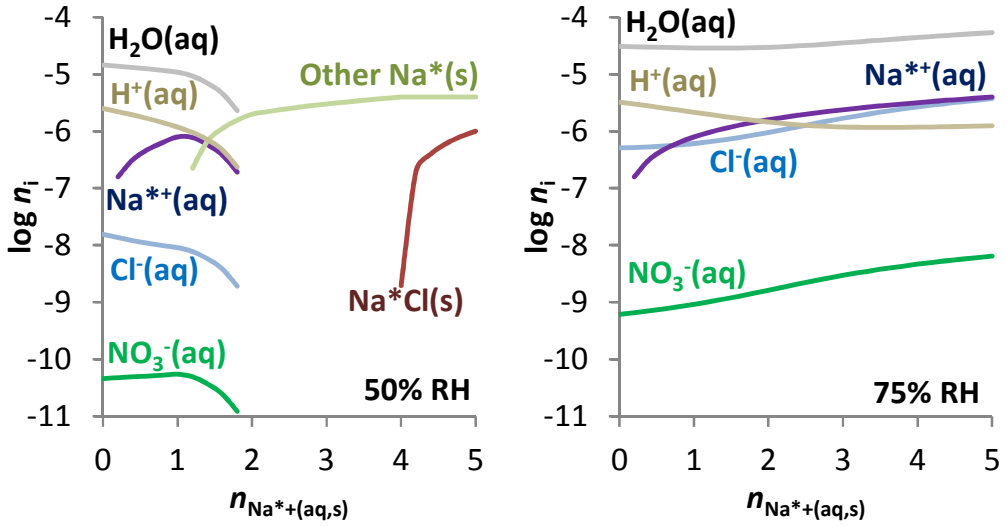

505 **FIGURE 4**

506 Three-parameter model results for equilibrium $a_{X(aq)}/p_{HX(g)}$ (with $a_{X(aq)}=a_{X\text{-}(aq)+}\ a_{HX(aq)}$) for the standard
507 input composition at 298 K, using parameters in Table 1. Equivalent results from E-AIM1 for Cl, Br
508 and NO_3 are shown with the approximation that $a_{HX(aq)}=0$. Also shown are results for $n_{Cl\text{-}(aq)}$, $n_{Br\text{-}(aq)}$,
509 $n_{NO3\text{-}(aq)}$ (in mol m^{-3} of air) from E-AIM1 for the standard input composition at 298 K, as a function of
510 the relative humidity. $n_{HF(aq)}$ and $n_{I\text{-}(aq)}$ are estimated as described in the text.

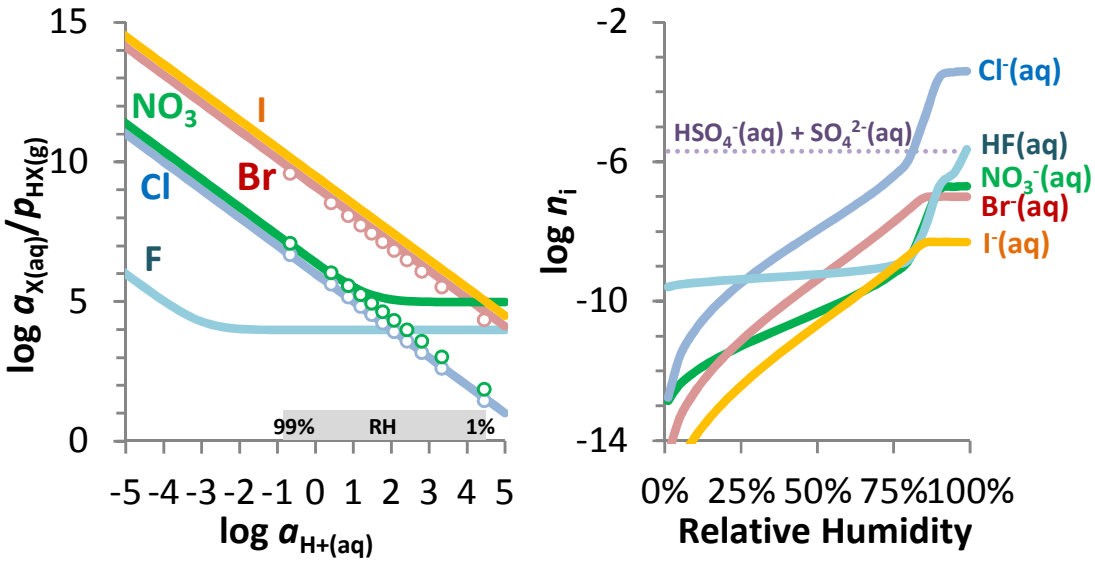

511

512

513